Research Square

Preprints are preliminary reports that have not undergone peer review.
They should not be considered conclusive, used to inform clinical practice,
or referenced by the media as validated information.

Phase-space visualization of global warming data

Michael Philipp Adams

michael.adams@mpsd.mpg.de

Max Planck Institute for the Structure and Dynamics of Matter

Article

Keywords:

Posted Date: November 2nd, 2026

DOI: https://doi.org/10.21203/rs.3.rs-11351600/v1

License: This work is licensed under a Creative Commons Attribution 4.0 International License.
Read Full License

Additional Declarations: No competing interests reported.

Phase-space visualization of global warming data

Michael P. Adams[1,2,*]

[1]Department of Physics and Materials Science, University of Luxembourg, 162a avenue de la Faïencerie, L-1511 Luxembourg, Luxembourg
[2]Present address: Max Planck Institute for the Structure and Dynamics of Matter, Luruper Chaussee 149, D-22761 Hamburg, Germany; Center for Free-Electron Laser Science, Notkestrasse 85, D-22607 Hamburg, Germany
[*]michael.adams@mpsd.mpg.de

ABSTRACT

Global mean surface temperature anomalies are commonly analyzed using trends, warming rates, and accelerations derived from one-dimensional time series. In this article we introduce a complementary geometric perspective by representing the historical temperature record in phase space. Using four major observational temperature datasets and multiple smoothing approaches, we reconstruct smooth temperature trends T together with their first and second temporal derivatives (T', T''), yielding trajectories in the three-dimensional (T, T', T'') phase space that jointly encode temperature level, warming rate, and acceleration. Across datasets and methods, the reconstructed trajectories exhibit a coherent large-scale geometric structure: an early loop-like excursion followed by a persistent drift-like regime in which both warming rate and acceleration occupy predominantly positive regions of phase space. Within the tested ensemble of regularized reconstructions, the observed phase-space structure is stable across dataset choice, smoothing framework, and parameter variation, indicating that it reflects a robust descriptive feature of the reconstructed temperature record rather than the outcome of a single smoothing procedure. These results show that phase-space representations make the joint organization of temperature, warming rate, and acceleration explicit, providing a compact and informative diagnostic for analyzing long-term climate evolution.

Introduction

The global mean surface temperature anomaly is one of the most widely used indicators of climate change, providing a compact summary of the integrated response of the climate system to natural variability and anthropogenic forcing[1–3]. Owing to its central role in climate assessment, the temperature record has been extensively analyzed using a variety of time-series-based approaches, including moving averages, regression-based trend estimates, polynomial fits, kernel smoothers, and stochastic filtering techniques[4–9]. These methods have been highly successful in quantifying long-term warming and associated uncertainties.

At the same time, conventional analyses typically treat temperature level, warming rate, and acceleration as separate diagnostic quantities. Trends, first derivatives, and second derivatives are often examined in isolation or over restricted time windows. While this decomposition is analytically convenient, it obscures how these quantities evolve jointly over the full observational record. As a result, potential large-scale structural features—such as regime-like behavior, transitions, or persistent organization in the combined evolution of temperature and its derivatives—may remain difficult to identify in purely one-dimensional representations.

Recent work has therefore emphasized the limitations of scalar summaries and local trend diagnostics. Studies have explored the spectral structure of temperature variability[10], the sensitivity of inferred trends to methodological choices[11], and evidence for changes in the rate or acceleration of global warming in recent decades[12–15], typically expressed through regression-based estimates of scalar acceleration measures, changes in warming rate, or time-resolved kinematic paths. In this context, it has become increasingly relevant to ask not only whether warming is accelerating, but how temperature level, warming rate, and acceleration organize jointly over time.

A natural way to make this joint evolution explicit is through a phase-space representation. In nonlinear dynamics, phase space methods are widely used to visualize system evolution, identify qualitative behavior, and characterize transitions without necessarily invoking a specific governing model[16–20]. By treating temperature and its temporal derivatives as coordinates of a single trajectory, a phase-space representation encodes temperature level, warming rate, and acceleration into a unified geometric object. This allows qualitative features—such as loop-like excursions, drift, or changes in trajectory orientation—to be identified at the level of global geometric organization rather than through pointwise trend estimates.

In this study, we introduce a complementary phase-space perspective on global surface temperature change by analyzing the trajectory formed by the temperature trend T and its first and second temporal derivatives (T', T'') in the three-dimensional space (T, T', T''). Here, the term phase space is used in a descriptive sense to denote the geometric embedding of the temperature record and its derivatives, without assuming an underlying low-dimensional dynamical system or governing equations. The focus is on the geometric structure of the reconstructed trajectory and its robustness, not on deriving or fitting a low-dimensional dynamical model. Terms such as "regime" are used here in a purely geometric sense, referring to distinct segments of the phase-space trajectory rather than to dynamical attractors or equilibria.

To assess the stability of the observed geometric features, we analyze four major observational global temperature datasets (NASA GISTEMP v4 (1880–2024)[2,21], Berkeley Earth (1850–2024)[3,22], HadCRUT5 non-infilled v5.0.2.0 (1850–2024)[23,24], and NOAA Global Surface Temperature v6 (90°S–90°N, land–ocean, 1850–2024)[25]) using a set of complementary smoothing frameworks. This ensemble-based approach allows us to test whether qualitative phase-space structures persist across datasets, smoothing methodologies, and parameter choices. Details of the smoothing frameworks, derivative estimation, and robustness analysis are provided in the Supplementary Methods.

Results

The central results of our analysis are presented in Figs. 1 and 2. Fig. 1 shows the ensemble-averaged phase-space trajectory, while Fig. 2 quantifies the associated empirical ensemble spread.

Fig. 1(a) shows the filtered global warming phase-space trajectory (T, T', T'') reconstructed using four major observational global temperature datasets and six complementary smoothing methods (see Methods). Here, T denotes the global temperature anomaly, $T' = dT/dt$ the warming rate (first time derivative), and $T'' = d^2T/dt^2$ the acceleration (second time derivative). Figs. 1(b–d) show projections of the three-dimensional phase-space trajectory onto the planes (b) T'–T, (c) T''–T', and (d) T''–T. Since time is an implicit parameter of the phase-space trajectory, the annual correspondence is color-coded and indicated by the colorbar spanning the period from 1880 to 2022. Although the original datasets extend to 2024, the phase-space trajectory is shown only up to 2022 because the use of forward finite differences for derivative estimation reduces the effective time range near the upper temporal boundary.

In addition to Fig. 1, Fig. 2 provides a robustness assessment. For each annual time step, it displays an empirical 3σ ensemble-spread ellipsoid in the (T, T', T'') phase space, constructed from an ensemble of phase space trajectories obtained using the four major observational datasets, six smoothing methods (see Methods), and a variation of filter parameters, resulting in a total of 140 trajectories. At each time step, the ellipsoid is defined by the empirical covariance matrix of the ensemble of phase space points, with its principal axes given by the eigenvectors of the covariance and semi-axis lengths proportional to $3\sqrt{\lambda_i}$, where λ_i denote the corresponding eigenvalues. The phase-space trajectory shown in Fig. 1 corresponds to the geometric centers of the empirical ensemble-spread ellipsoids at each time step.

Fig. 2 shows increased variability near the temporal boundaries, approximately in the ranges 1880–1900 and 2012–2022. This behavior is expected for fit-based analyses, as no earlier or future data are available to constrain the fits near the respective temporal boundaries. Consequently, different smoothing methods diverge more strongly at the lower and upper temporal boundaries, and the associated ensemble spread is expected to decrease as additional future observations become available. Furthermore, Fig. 2 indicates that the variability of the trajectories is anisotropic across the phase space coordinates: the empirical ensemble-spread ellipsoids are comparatively narrow along T, reflecting greater stability and agreement across the reconstructed temperature trajectories, while the spread increases with increasing derivative order from T to T'', relative to the corresponding value ranges of these quantities. This anisotropic behavior is expected because temporal differentiation amplifies relative variations, making higher-order derivatives more sensitive to reconstruction choices than the underlying observable.

Together, Figs. 1 and 2 illustrate a robust change in the geometric structure of the (T, T', T'') phase-space trajectory, evolving from an initially loop-like (or weakly spiral-like) configuration to a predominantly line- or drift-like geometry. In addition to the three-dimensional representations in Figs. 1(a) and 2(a), the two-dimensional projections in Figs. 1(b) and (c) highlight this behavior more clearly: Fig. 1(b) displays a partial loop followed by a drift-like regime in the T'–T plane, and Fig. 1(c) shows an initial loop turning into a path that remains in the positive quadrant of the T''–T' plane. In addition, Fig. 1(d) shows an initially oscillatory relation between T'' and T, including zero-crossings of T'', that transitions into a trajectory confined to the positive quadrant of the T''–T plane.

As a compact descriptive check of the ensemble, rather than as a formal acceleration-detection test, we also evaluated the sign structure of the reconstructed phase-space points. Over the period 2005–2019, all ensemble points represented in this interval have positive warming rate $T' > 0$, and approximately 90% also lie in the positive T'' region. The empirical ensemble center remains in the positive T'–T'' quadrant throughout this interval. These fractions should be read as summaries of the tested regularized reconstruction ensemble, not as probabilities for the true annual acceleration.

For completeness, the associated Zenodo repository[26] contains two videos illustrating the time evolution of the phase space trajectories shown in Figs. 1 and 2, including annual time-stamp labels for each data point.

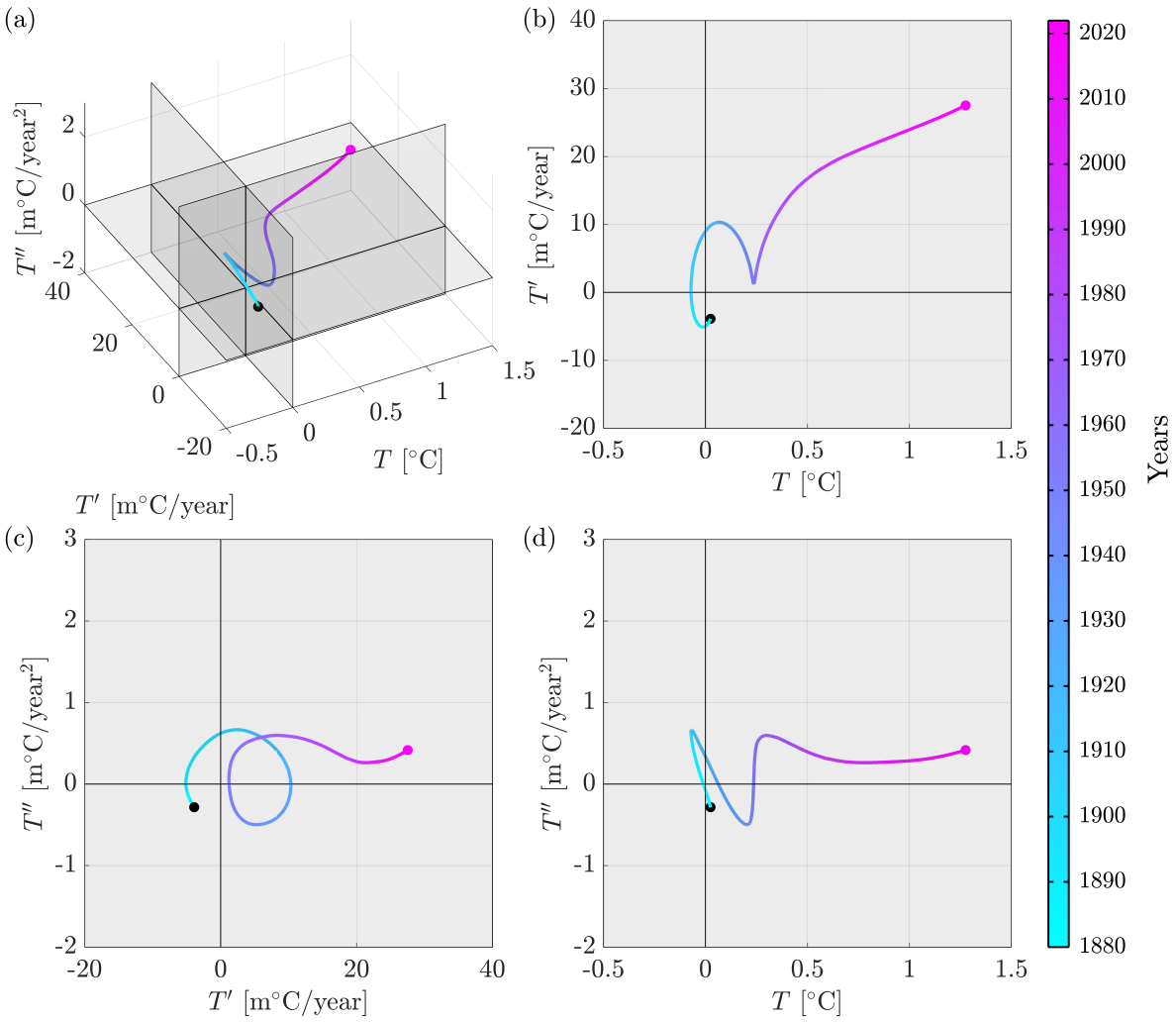


Figure 1. Average phase-space trajectory of global warming in the (T, T', T'') space. Phase-space reconstruction of the global annual mean surface temperature anomaly, illustrating the qualitative geometric evolution of the temperature record. The trajectory exhibits an initial loop-like regime, followed by a persistent positive-drift regime. Colors indicate calendar year. Derivative axes are reported in m°C/year and m°C/year^2, where m°C denotes 10^{-3} °C. This representation highlights the large-scale geometric form and direction of climate evolution and displays the ellipsoid centers of the robustness analysis shown in Fig. 2. The trajectories should be interpreted as regularized diagnostic reconstructions rather than as pointwise annual estimates. In particular, the sign and magnitude of T'' near the temporal boundaries, including the most recent years, are more sensitive to the reconstruction method, as reflected by the increased ensemble spread in Fig. 2(c,d).

Discussion

This study introduces a phase-space perspective on global surface temperature anomalies by analyzing the joint evolution of the temperature T and its first and second temporal derivatives T' and T''. Rather than focusing on individual trend or acceleration estimates derived from regression-based analyses, this approach emphasizes geometric features of the trajectory in (T, T', T'')-space that summarize the long-term organization of global warming in a compact geometric manner.

Across four observational datasets and six smoothing methods, a consistent qualitative structure emerges. In the early part of the record, the phase-space trajectory exhibits a loop-like configuration, with oscillatory behavior of T' and T'' including zero-crossings. From the mid-twentieth century onward, this behavior transitions into a persistent drift-like regime in which both the warming rate and acceleration occupy predominantly positive regions of phase space. Although the precise shape of the trajectory depends on the smoothing framework, this large-scale geometric organization remains stable within the tested

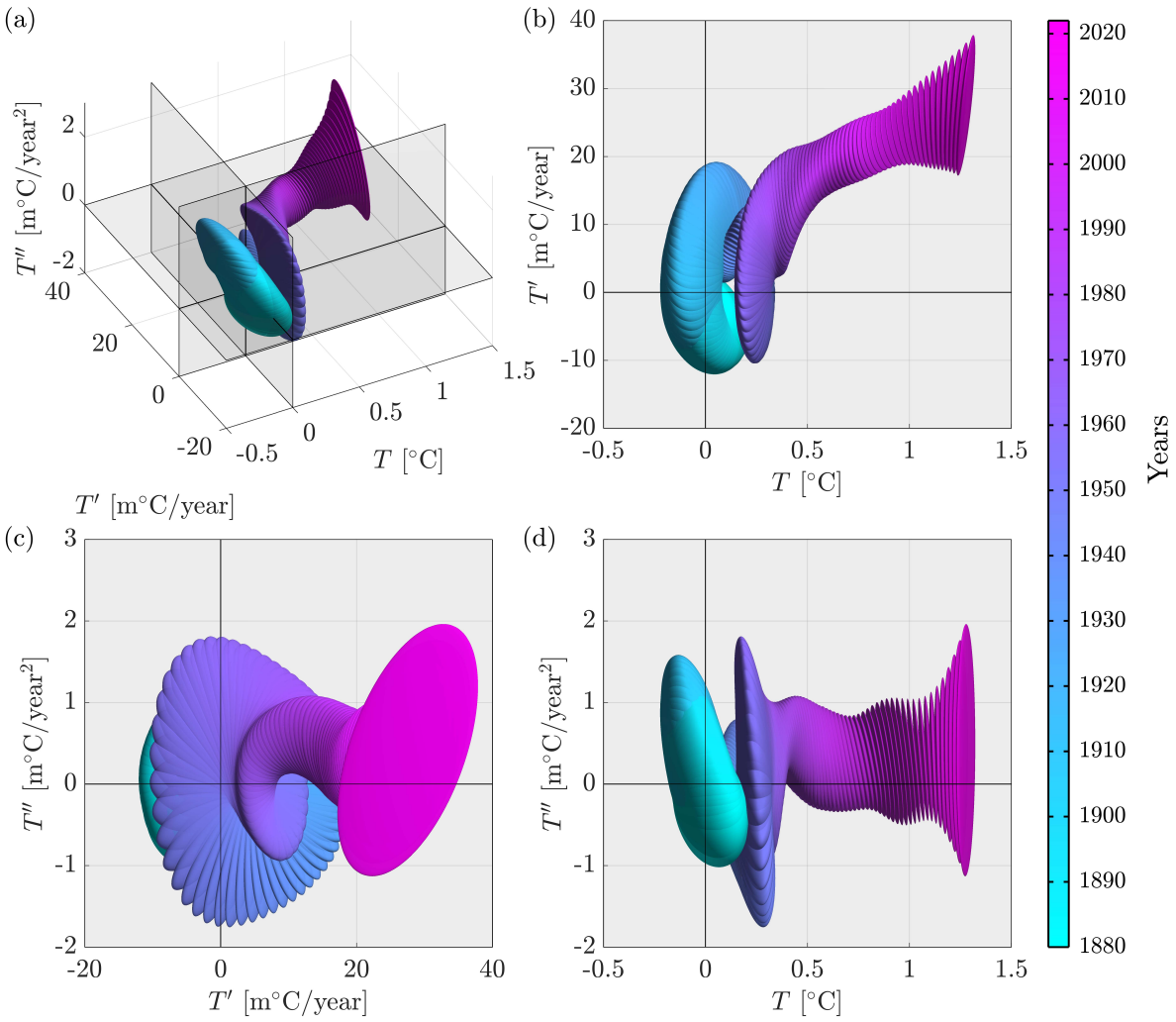


Figure 2. Phase-space structure across datasets, methods, and parameter choices. The figure shows local empirical 3σ ensemble-spread ellipsoids in the (T, T', T'') phase space, constructed at each time step from the empirical covariance of an ensemble of phase space points obtained across four major observational global temperature datasets, six smoothing methods, and parameter variations. The ellipsoids quantify methodological and dataset-induced variability in the reconstructed temperature T and its derivatives (T', T''), rather than statistical measurement uncertainty or exhaustive confidence regions over all possible smoothing choices. The geometric centers of the ellipsoids define the average phase-space trajectory shown in Fig. 1.

combination of datasets, methods, and parameter choices. This consistency supports its interpretation as a feature of the temperature record rather than as a structure imposed by any single reconstruction method.

In the context of ongoing discussions about the detectability and statistical significance of warming acceleration[12–14,27], it is important to distinguish between formal inference on a single interval-wide acceleration parameter and structural consistency of a time-resolved regularized trajectory. From a kinematic and geometric perspective, trajectory segments in which the warming rate T' itself increases cannot be generated by a purely zero-acceleration reconstruction over the same interval, while persistently negative acceleration would imply a sustained decline in T'. The present analysis, however, does not aim to estimate or formally test a specific interval-wide acceleration parameter. In this sense, T'' is not interpreted as a sequence of independent annual acceleration estimates, but as one coordinate of a regularized geometric embedding in which the relevant information lies in the organization and orientation of the trajectory as a whole. The relevant object of interpretation is therefore not the annual value of T'' at an isolated time point, but the persistence, orientation, and deformation of the reconstructed trajectory under changes of dataset and smoothing framework.

A complementary detectability analysis by Beaulieu et al. applied continuous and discontinuous piecewise-linear change-point models with autoregressive residuals to the same four major GMST records through 2023[27]. No statistically detectable post-1970 change in warming rate was found. Across the four datasets, an increase of at least 55% was estimated to be necessary for a warming surge to be detectable at the 2024 vantage point. The authors emphasized that the absence of detection does not exclude a change that is too small or too recent to distinguish from short-term variability. Their result concerns formal evidence for a change in linear trend and is therefore compatible with descriptive geometric changes in a regularized trajectory that are not interpreted as change-point detection.

For external scale comparison, Richardson's unadjusted quadratic regressions over 1980–2020 yielded a mean acceleration of $49\,\mathrm{m^{\circ}C\,decade^{-2}}$ across the latest versions of the three principal datasets used in the IPCC Fifth Assessment Report. After accounting for ENSO, volcanic aerosols, and solar variability, the across-dataset mean of the adjusted fits was $36\,\mathrm{m^{\circ}C\,decade^{-2}}$, with a mean $2\sigma_c$ range of $\pm 30\,\mathrm{m^{\circ}C\,decade^{-2}}$. Large-ensemble tests further indicated that several standard approaches underestimated uncertainty and that an acceleration of $49\,\mathrm{m^{\circ}C\,decade^{-2}}$ would likely not be detectable with robust confidence until at least 2026 under the assumptions of that analysis[12]. In the units used here, the two central estimates correspond to $0.49\,\mathrm{m^{\circ}C\,year^{-2}}$ and $0.36\,\mathrm{m^{\circ}C\,year^{-2}}$, respectively, and the adjusted mean range corresponds to $\pm 0.30\,\mathrm{m^{\circ}C\,year^{-2}}$. These interval-wide estimates provide an external scale reference for the reconstructed T'' values in Fig. 1(c,d), but not an independent validation: the analyses partly rely on the same observational records and quantify different sources of uncertainty.

More recent work by Foster and Rahmstorf applied two distinct formal tests to five GMST datasets after empirical adjustment for ENSO, volcanic aerosols, and solar variability: a quadratic model and a continuous piecewise-linear model with an objectively selected change point[14]. Both tests rejected a constant post-1970 warming rate for the adjusted records, but the inferred recent warming-rate histories differed substantially between the two models. Moving ten-year regressions agreed more closely with the piecewise-linear reconstruction; the change-point model located changes in slope around 2013–2014. Their comparison therefore provides a methodological reference for the model dependence of reconstructed warming-rate histories. The present analysis does not reproduce their formal change-point test; it examines geometric changes in the joint T, T', and T'' trajectory across smoothing frameworks and parameter choices.

A closely related kinematic analysis by Bennedsen and Vera-Valdés jointly estimates latent warming level, warming rate, and acceleration from five global temperature records using a semiparametric state-space framework and compares the resulting paths with nonparametric and parametric estimators[15]. Their results likewise emphasize that inferred recent warming dynamics, particularly acceleration, depend on the estimated quantity and estimator class. Whereas that analysis presents the three kinematic quantities primarily as time-resolved paths, the present study treats their joint geometry in (T, T', T'')-space as the object of interest and evaluates its persistence across smoothing frameworks and parameter choices.

The three-dimensional reconstruction in (T, T', T'')-space highlights these features at the level of global geometric organization. The trajectory traces a loop-like, weakly spiral geometry in the early decades before evolving into a smoother, monotonically drifting path. These structures should be interpreted as descriptive properties of the temperature time series rather than as indicators of underlying physical mechanisms. Their primary value lies in providing a compact visual summary of how temperature level, warming rate, and acceleration evolve jointly over the observational record.

Because the phase-space representation does not assume a specific governing climate model, but does rely on regularized reconstruction of T, T', and T'', it is best viewed as a complementary diagnostic rather than a predictive tool. It can be used to compare observational datasets, assess robustness across reconstruction methods, and evaluate whether climate model simulations reproduce similar geometric features over the historical period. Extensions to multivariate embeddings, regional temperature records, higher-resolution datasets, or alternative reconstruction frameworks may further clarify the spatial and temporal structure of the observed phase-space organization.

In summary, the phase-space perspective offers a concise and robust way to visualize the joint evolution of temperature, warming rate, and acceleration across observational datasets. By focusing on geometric structure rather than isolated scalar diagnostics, it complements conventional time-series analyses and provides an additional lens through which long-term climate evolution can be examined.

Methods

We analyzed four major observational global surface temperature anomaly datasets: NASA GISTEMP v4 (1880–2024)[2,21], Berkeley Earth (1850–2024)[3,22], HadCRUT5 non-infilled v5.0.2.0[23,24], and NOAA Global Surface Temperature v6 (90°S–90°N, land–ocean)[25]. All records were reduced to annual means. To facilitate a consistent geometric comparison across datasets, the temperature anomaly series were temporally aligned and adjusted by removing dataset-specific offsets through centering and a shared reference interval (1880–1940). This alignment affects only the absolute temperature level T, while temporal derivatives and the phase space geometry of the reconstructed trajectories remain invariant under constant offsets. The harmonized annual temperature anomaly time series used in this study are shown in `fig0.png` of the associated Zenodo repository[26].

To reconstruct smooth temperature trends T and their first and second temporal derivatives (T', T''), we employed a set of complementary smoothing approaches designed to stabilize derivative estimation while preserving long-term structure. For illustrative purposes, an example comparison of the reconstructed temperature trends and their first and second temporal derivatives obtained with different smoothing methods for a representative parameter choice is shown in `fig1.png` of the associated Zenodo repository[26].

To assess methodological robustness, the analysis was repeated using six smoothing frameworks spanning different methodological families: a multilayer moving-average filter, Fourier–Sobolev smoothing, Legendre–Sobolev smoothing, finite-difference Sobolev filtering, Gaussian process regression, and the Heisenberg-Regularized Anisotropic Gaussian (HRAG) trend estimator. Together, these methods encompass both parametric and nonparametric approaches, spectral and time-domain formulations, and deterministic as well as probabilistic smoothers.

An initial pre-selection also included LOWESS smoothing. However, LOWESS was excluded from the final ensemble because its locally adaptive weighting scheme leads to unstable estimates of first- and second-order derivatives, particularly near data-sparse regions and temporal boundaries. Since the focus of this study is on robust phase space geometry involving derivatives up to second order, LOWESS was not considered further and does not contribute to the results shown in the main figures. For completeness, LOWESS-based analyses are documented in the associated data repository.

For each dataset and smoothing method, parameter sweeps were performed over broad method-specific ranges to generate ensembles of trend trajectories and corresponding phase space curves. The regularization parameters are not interpreted as uniquely determined by the data; rather, they define a class of admissible smooth reconstructions in which ill-conditioned high-frequency derivative noise is suppressed while large-scale phase-space features are retained. Derivatives were computed using forward finite differences with a fixed annual time step. Local empirical 3σ ensemble-spread ellipsoids in phase space were obtained from the ensemble variability at each time step and are used to quantify methodological and dataset-related variability.

Finally, we emphasize that derivative reconstruction from finite, noisy temperature records is intrinsically sensitive to smoothing choices, and that the estimation of second-order derivatives is particularly ill-conditioned. The present analysis should therefore be interpreted as a regularized reconstruction of phase-space geometry rather than as a direct differentiation of the raw records. To assess whether the resulting qualitative structure depends on a specific reconstruction choice, we repeated the analysis across multiple smoothing frameworks and regularization parameters. Within the resulting ensemble spread, the large-scale transition from an early loop-like configuration to a drift-like regime remains qualitatively stable.

Full methodological descriptions, parameter values, sensitivity analyses, and reproducibility materials are provided in the associated Zenodo repository[26].

Data Availability

The four global surface temperature anomaly datasets analyzed in this study are publicly available:

- NASA GISTEMP v4 Land–Ocean Temperature Index (LOTI), covering 1880–2024[2,21];
- Berkeley Earth global land–ocean temperature data, covering 1850–2024[3,22];
- HadCRUT5 non-infilled version 5.0.2.0, covering 1850–2024[23,24]; and
- NOAA Global Surface Temperature version 6, land–ocean, 90°S–90°N, covering 1850–2024[25].

The source snapshots used in the analysis, the harmonized annual series, processed trend and trajectory data, trajectory metadata, MATLAB analysis code, and reproducibility materials are archived in the versioned Zenodo repository[26].

References

1. IPCC. Climate change 2021: The physical science basis. contribution of working group i to the sixth assessment report of the intergovernmental panel on climate change. https://www.ipcc.ch/report/ar6/wg1/, DOI: 10.1017/9781009157896 (2021). ISBN: 9781009157896, Accessed: 2024-07-01.
2. NASA Goddard Institute for Space Studies. Gistemp v4: Nasa global surface temperature analysis. https://data.giss.nasa.gov/gistemp/graphs_v4/ (2024). Accessed: 2024-06-30.
3. Earth, B. Global temperature report for 2024. https://berkeleyearth.org/global-temperature-report-for-2024/ (2024). Accessed: 2024-07-01.
4. Rahmstorf, S. *et al.* Recent climate observations compared to projections. *Science* **316**, 709–709, DOI: 10.1126/science.1136843 (2007).

5. Hansen, J. *et al.* Global temperature change. *Proc. Natl. Acad. Sci.* **103**, 14288–14293, DOI: 10.1073/pnas.0606291103 (2006).

6. Hansen, J., Ruedy, R., Sato, M. & Lo, K. Global surface temperature change. *Rev. geophysics* **48**, DOI: 10.1029/2010RG000345 (2010).

7. Zhou, J. & Tung, K.-K. Deducing multidecadal anthropogenic global warming trends using multiple regression analysis. *J. Atmospheric Sci.* **70**, 3–8, DOI: 10.1175/JAS-D-12-0208.1 (2013).

8. Haustein, K. *et al.* A real-time global warming index. *Sci. Reports* **7**, 15417, DOI: 10.1038/s41598-017-14828-5 (2017).

9. Clarke, D. C. & Richardson, M. The benefits of continuous local regression for quantifying global warming. *Earth Space Sci.* **8**, e2020EA001082, DOI: 10.1029/2020EA001082 (2021).

10. Tenreiro Machado, J. & Lopes, A. M. Dynamical analysis of the global warming. *Math. Probl. Eng.* **2012**, 971641, DOI: 10.1155/2012/971641 (2012).

11. De Saedeleer, B. Climatic irregular staircases: generalized acceleration of global warming. *Sci. Reports* **6**, 19881, DOI: 10.1038/srep19881 (2016).

12. Richardson, M. T. Prospects for detecting accelerated global warming. *Geophys. Res. Lett.* **49**, e2021GL095782, DOI: 10.1029/2021GL095782 (2022).

13. Hansen, J. E. *et al.* Global warming has accelerated: Are the united nations and the public well-informed? *Environ. Sci. Policy for Sustain. Dev.* **67**, 6–44, DOI: 10.1080/00139157.2025.2434494 (2025).

14. Foster, G. & Rahmstorf, S. Global warming has accelerated significantly. *Geophys. Res. Lett.* **53**, e2025GL118804, DOI: 10.1029/2025GL118804 (2026).

15. Bennedsen, M. & Vera-Valdés, J. E. The kinematics of global warming: Semiparametric analysis of warming level, rate, and acceleration, DOI: 10.48550/arXiv.2608.18298 (2026). 2608.18298.

16. Packard, N. H., Crutchfield, J. P., Farmer, J. D. & Shaw, R. S. Geometry from a time series. *Phys. Rev. Lett.* **45**, 712–716, DOI: 10.1103/PhysRevLett.45.712 (1980).

17. Guckenheimer, J. & Holmes, P. *Nonlinear Oscillations, Dynamical Systems, and Bifurcations of Vector Fields* (Springer, New York, 1983), DOI: 10.1007/978-1-4612-1140-2.

18. Ott, E. *Chaos in Dynamical Systems* (Cambridge University Press, 2002), DOI: 10.1017/CBO9780511803260.

19. Kantz, H. & Schreiber, T. *Nonlinear Time Series Analysis: Second Edition* (Cambridge University Press, 2004), DOI: 10.1017/CBO9780511755798.

20. Strogatz, S. H. *Nonlinear Dynamics and Chaos: With Applications to Physics, Biology, Chemistry, and Engineering* (Westview Press, Boulder, CO, 2015), 2nd edn.

21. Lenssen, N. *et al.* A gistempv4 observational uncertainty ensemble. *J. Geophys. Res. Atmospheres* **129**, e2023JD040179, DOI: 10.1029/2023JD040179 (2024).

22. Rohde, R. A. & Hausfather, Z. The berkeley earth land/ocean temperature record. *Earth Syst. Sci. Data* **12**, 3469–3479, DOI: 10.5194/essd-12-3469-2020 (2020).

23. Morice, C. *et al.* An updated assessment of near-surface temperature change from 1850: The hadcrut5 data set. *J. Geophys. Res. Atmospheres* **126**, e2019JD032361, DOI: 10.1029/2019JD032361 (2020).

24. Met Office Hadley Centre & Climatic Research Unit, University of East Anglia. HadCRUT5 global surface temperature dataset. https://crudata.uea.ac.uk/cru/data/temperature/ (2021). Version 5.0.2.0 (non-infilled), accessed 2025-12-01.

25. Yin, X. *et al.* Noaaglobaltemp version 6: An ai-based global surface temperature dataset. *Bull. Am. Meteorol. Soc.* **105**, E2184 – E2193, DOI: 10.1175/BAMS-D-24-0012.1 (2024).

26. Adams, M. P. Phase-space structure of global warming. Zenodo, DOI: 10.5281/zenodo.17447485 (2025).

27. Beaulieu, C., Gallagher, C., Killick, R., Lund, R. & Shi, X. A recent surge in global warming is not detectable yet. *Commun. Earth & Environ.* **5**, 576, DOI: 10.1038/s43247-024-01711-1 (2024).

Author contributions statement

M.A. conceived the study, conducted the analysis, developed the methodology, generated all figures, and wrote the manuscript.

Funding Declaration

No funding was received for this research.

Additional information

Competing interests. The author declares no competing interests.

Supplementary Files

This is a list of supplementary files associated with this preprint. Click to download.

- methods.pdf